

Article

## NANOPARTICLES LOADED WITH PROCYANIDIN B2-3'-O-GALLATE FROM GRAPE SEED: PREPARATION, CHARACTERIZATION AND ANTIOXIDANT ACTIVITY

### NANOPARTÍCULAS CONTENDO PROCIANIDINA B2-3'-O-GALHATO DE GRAINHA DE UVA: PREPARAÇÃO, CARACTERIZAÇÃO E ATIVIDADE ANTIOXIDANTE

Wenxin Wu<sup>1</sup>, Shuting Zhang<sup>2</sup>, Yuanyuan Tang<sup>2</sup>, Xiangrong Zhang<sup>2,\*</sup>, Baoshan Sun<sup>2,3,\*</sup>

<sup>1</sup>School of Traditional Chinese Materia Medica, Shenyang Pharmaceutical University, 110016 Shenyang, China.

<sup>2</sup>School of Functional Food and Wine, Shenyang Pharmaceutical University, 110016 Shenyang, China.

<sup>3</sup>Instituto Nacional de Investigação Agrária e Veterinária, Polo de Inovação de Dois Portos, Quinta da Almoinha, 2565-191 Dois Portos, Portugal.

\*Corresponding authors: Tel:86-24-43520300; email: zhangxr@vip.sina.com; sun.baoshan@iniav.pt

(Received date 13.02.2023. Accepted date 26.05.2023)

#### SUMMARY

The aim of this study was to prepare nanoparticles of grape seed procyanidin B2-3'-O-gallate by chitosan-sodium alginate. The encapsulation system was characterized by transmission electron microscope (TEM), Fourier transform infrared spectroscopy (FTIR), X-ray diffraction (XRD) and differential scanning calorimetry (DSC), and its biological activity was analyzed by cell-level antioxidant capacity. The results showed that the particle size of nano-carrier was 160~201nm, the B2-3'-O-gallate was well embedded, and the encapsulation efficiency of B2-3'-O-gallate was 93.5%. *In vitro* digestion experiments suggested that the release of B2-3'-O-gallate was significantly controlled by chitosan-sodium alginate nano-system through anomalous diffusion mechanism, and at about 72-78% of B2-3'-O-gallate was retained under gastrointestinal (GI) condition. Besides, the cytotoxicity results expressed that B2-3'-O-gallate chitosan nanoparticles had obvious protective effect on human HepG2 cells induced by hydrogen peroxide. This work provides a promising way to control the delivery and enhances the biological activity of galloylated procyanidins – one of the most important group of bioactive polyphenols of the grape pomace.

#### RESUMO

O objetivo deste estudo foi preparar nanopartículas de procianidina B2-3'-O-galhato de grainhas de uva através do quitosano-alginato de sódio. O sistema de encapsulação foi caracterizado por microscópio eletrónico de transmissão (TEM), espectroscopia de infravermelho com transformada de Fourier (FTIR), difração de raios X (XRD) e calorimetria exploratória diferencial (DSC), e sua atividade biológica foi analisada pela capacidade antioxidante ao nível celular. Os resultados mostraram que o tamanho da partícula do nanoencapsulador era de 160~201 nm, a B2-3'-O-galhato estava bem incorporada, e a eficiência de encapsulação de B2-3'-O-galhato foi de 93,5%. Ensaios de digestão *in vitro* sugeriram que a libertação de B2-3'-O-galhato foi significativamente controlada pelo nanossistema quitosana-alginato de sódio através de um mecanismo de difusão anómalo, e cerca de 72-78% de B2-3'-O-galhato foi retida sob condição gastrointestinal (GI). Por outro lado, os resultados de citotoxicidade indicaram que as nanopartículas de quitosana de B2-3'-O-galhato tiveram um efeito protetor óbvio em células humanas HepG2 induzidas por peróxido de hidrogénio. Este trabalho apresenta um processo promissor para controlar a disponibilização e aumentar a atividade biológica de procianidinas galhoiladas – um dos grupos mais importantes de polifenóis bioativos do bagaço de uva.

**Keywords:** Grape seed, procyanidin B2-3'-O-gallate, chitosan-sodium alginate, nanoparticles, antioxidant activity.

**Palavras-chave:** Grainha de uva, procianidina B2-3'-O-galhato, quitosana-alginato de sódio, nanopartículas, atividade antioxidante.

© Wu *et al.*, 2023.

This is an Open Access article distributed under the terms of the Creative Commons Attribution License (<https://creativecommons.org/licenses/by/4.0>), which permits unrestricted use, distribution, and reproduction in any medium, provided the original work is properly cited

## INTRODUCTION

Grape pomace, a by-product of winemaking, is a rich source of polyphenols, particularly proanthocyanidins (Sun *et al.*, 2001, 2005). Proanthocyanidins (PCs) are a class of polyphenol compounds, especially oligomeric proanthocyanidins (OPCs), which have a variety of biological activities (Bitzer *et al.*, 2015). The galloylated proanthocyanidins are a kind of polyphenols with galloylated groups inserted into their chemical structure. Studies showed that galloylated proanthocyanidins had significantly higher biological activities than the non-galloylated ones (Agarwal *et al.*, 2007; Suda *et al.*, 2013; Tyagi *et al.*, 2014). However, the structures such as polyhydroxy and unsaturated bonds in the galloylated proanthocyanidins generally lead to poor chemical stability, high sensitivity, short biological half-life, low bioavailability and susceptibility to oxidative degradation (Rajapaksha and Shimizu, 2020).

As chitosan nanoparticles can stabilize the bioactive components and improve the activity of the coating substances, the preparation of nanoparticles based on chitosan material has become one of the hot spots in recent years (Gao and Wu, 2022). Methods for preparing the chitosan nanoparticles include ion crosslinking, emulsion, carboxymethyl cellulose synthesis, glutaraldehyde crosslinking, alginic acid synthesis, coagulation, reverse micelle, 2-hydroxyethyl methacrylate polymerization (Hua *et al.*, 2021). Because sodium alginate is nontoxic and convenient and has no chemical reagent residue, the ion crosslinking technology is most widely used (Jadach *et al.*, 2022).

In addition, due to their small diameter, chitosan nanoparticles could penetrate tumor tissue through its vascular endothelial slits and accumulate high concentrations in this region over a long period of time by enhancing permeability and retention (EPR) effects due to inadequate venous and lymphatic clearance (Lopes *et al.*, 2017). Furthermore, the chitosan has a positive charge and interacts with the negatively charged cell membrane to promote structural disorder and increase the mobility of the membrane, which is beneficial to cell absorption (Karavelioglu and Cakir-Koc, 2021). The chitosan-based material is also very sensitive to exposure of weak acidic media (such as tumor microenvironment and internal lysosomal organelles), which can promote the release of active molecules in tumor microenvironment and cells (Sathiyaseelan *et al.*, 2020).

In this work, B2-3'-*O*-gallicate (B2-3'-G), the most important galloylated proanthocyanidin dimer isolated from grape seeds, was encapsulated into nanoparticles by ion crosslinking, in order to overcome the application limitations of the natural active products of galloylated proanthocyanidin such as poor physicochemical stability, high environmental sensitivity, among others, and to improve its biological activity. B2-3'-G chitosan-sodium alginate nanoparticles (ALG/CS-B-NPs) were prepared and characterized by transmission electron microscopy (TEM), Fourier transform infrared spectroscopy (FTIR), X-ray diffraction (XRD) and differential scanning calorimetry (DSC). The controlled release behavior of B2-3'-G was investigated under simulated gastrointestinal (GI) conditions, and its release kinetics were verified by multiple release mathematical models. Besides, human HepG2 cells were used in the *in vitro* cytotoxicity and cell uptake experiments. The protective effects of B2-3'-G and its chitosan-sodium alginate nanoparticles on H<sub>2</sub>O<sub>2</sub>-induced human HepG2 cell injury were also studied.

## MATERIALS AND METHODS

### Materials

B2-3'-G (HPLC purity > 98%) was prepared from grape seeds according to the method proposed in a previous work (Luo *et al.*, 2018). Sodium alginate (viscosity: 200 ± 20 mPa.s) was obtained from Shanghai Macklin Biochemical Technology Co., Ltd. (Shanghai, China). Chitosan (degree of deacetylation: 85%; molecular weight: 50 kDa; lot number: S24914) was purchased from Sinopharm Chemical Reagent Co. Ltd., (Shanghai, China). Pepsin (1:3000 NF) and pancreatin (100-350 U/mg) were supplied from Shanghai Aladdin Biotechnology Co., Ltd. (Shanghai, China). 3-(4,5-dimethyl-2-thiazolyl)-2,5-diphenyl-2-H-tetrazolium bromide (MTT), 2,2'-azino-bis-(3-ethylbenzothiazoline-6-sulfonic acid) diammonium salt (ABTS) were purchased from Sigma-Aldrich Co., Ltd. (St. Louis, USA). Fluorescein 5-isothiocyanate (FITC), 4',6-diamidino-2-phenylindole (DAPI) were supplied by Shanghai Macklin Biochemical Technology Co., Ltd. (Shanghai, China).

### Preparation of B2-3'-G alginate/chitosan nanoparticles

Sodium alginate/chitosan nanoparticles loaded with B2-3'-G (ALG/CS-B-NPs) were prepared by ion gel method (Marcato *et al.*, 2013). Briefly, chitosan (CS) solution (1 mg/mL) and sodium alginate (ALG) solution (1 mg/mL) were prepared, and the pH was adjusted to 4.5. Then a CS solution containing B2-

3'-G (0.5 mg/mL) was prepared, and it was dropwise added into the ALG solution under magnetic stirring, with the ratio of 1.2 or 0.2 (CS solution: ALG solution). Meanwhile, sodium alginate/chitosan nanoparticles containing no B2-3'-G were prepared as described above.

#### **Determination of encapsulation efficiency (EE)**

Encapsulation efficiency (EE) was determined using ultrafiltration technique (Ezzat *et al.*, 2019). The encapsulated B2-3'-G was separated by centrifugation at 3000g for 15 min at room temperature. The content of B2-3'-G in the supernatant was determined by sulfuric acid-vanillin method, and the absorbance at 500 nm was determined by microplate reader with methanol as the blank control (B2-3'-G Standard curve:  $y=1.7418x-0.026$ ,  $R^2=0.9995$ ). The EE (%) was calculated according to Equation 1.

$$EE\% = \frac{\text{Total amount of drug} - \text{amount untrapped}}{\text{Total amount of drug}} * 100 \quad \text{Eq. 1}$$

#### **Particle size, polydispersity index, and zeta potential**

The particle size and zeta potential were measured by a Zetasizer Nano ZS90 (Malvern Instruments Ltd., Malvern, UK). An appropriate amount of the diluted nanoparticle suspension was loaded into specific cuvette. Zeta potential determination steps were similar to the aforementioned method, the potential test special sample pool, carefully remove the nanoparticle suspension in the sample pool to avoid the generation of bubbles. Each sample was measured three times and the average value was calculated.

#### **Transmission electron microscopy (TEM)**

The morphologic characteristics of nanoparticles were monitored by transmission electron microscopy (TEM) (JEM-F200; JEOL Ltd., Tokyo, Japan). Samples of nanoparticle suspensions (5  $\mu$ L) were dropped onto Formvar-coated copper grids and stained using phosphotungstic acid (2% w/v).

#### **Fourier-transformed infrared spectroscopy (FTIR) analysis**

FTIR spectra were obtained using an FTIR spectrometer (FTIR-650, Guangdong, China). The samples (B2-3'-G, ALG, CS, and ALG/CS-B-NPs) were lyophilized, mixed with potassium bromide (KBr), ground to a fine powder, and manually pressed into KBr discs. Infrared spectra were obtained in the range of 500-4000  $\text{cm}^{-1}$ .

#### **X-ray diffraction (XRD) analysis**

The pure compound and the lyophilized polymeric nanoparticles were evaluated in an X-ray diffractometer model Ultima IV (Rigaku – Tokyo,

Japan) to assess their crystallinity pattern. The test parameters were set as tube current of 40 mA, scan rate of 5°/minute, scanning region of 2 $\theta$  from 5° to 90°, and using copper (Cu) as source.

#### **The thermogravimetric-differential scanning calorimetry (TG-DSC) analysis**

Thermal analyses of the samples were conducted by thermogravimetry and differential scanning calorimetry (TG-DSC, Netzsch STA449F3, Selb, Germany), under nitrogen atmosphere at a heating rate of 10 °C/min from 30 °C to 500 °C.

#### **In vitro simulated gastrointestinal digestion**

B2-3'-G and ALG/CS-B-NPs digestion were carried out under simulated gastric fluid (SGF) and simulated intestinal fluid (SIF). Samples were diluted with deionized water (1:4 v:v) for digestion. Prior to SGF digestion, 10 mL of the diluted samples were taken and adjusted to pH 2.0 using 5 M HCl, followed by the addition of 0.2 mg/mL porcine pepsin (1:3000 NF). The mixture was shaken in a 37 °C water bath shaker for 120 min. Subsequently, 0.2 mg/mL pancreatin (100-350 U/mg) was added, and the pH was adjusted to 7.4 with 1 M NaOH to simulate SIF digestion. In general, pancreatic enzymes remain activated at pH 7.4. Then, the mixture was incubated in a water bath chamber with mild shaking at 37 °C for 120 min. The samples were taken at a predetermined time (Li *et al.*, 2018; Shishir *et al.*, 2020).

#### **Determination of antioxidant activity before and after digestion**

To evaluate antioxidant activity before and after digestion, DPPH and FRAP assays were performed. The antioxidant activities of samples B2-3'-G and ALG/CS-B-NPs before and after digestion were compared. After gastrointestinal digestion, each sample was centrifuged for 10 min at 10,000g, and the supernatant was taken to evaluate the antioxidant activity retained in the carrier system.

DPPH is a stable free radical that is violet in the alcohol solution and have a maximum absorption at 517 nm. The single electron on the N atom of DPPH radical paired with the antioxidant makes the solution lose its color and the absorbance value decrease. The smaller the absorbance value, the stronger the antioxidant capacity to remove DPPH radical, that is, the stronger the antioxidant activity. Therefore, the ability of antioxidants to remove free radicals can be represented by the change in absorbance to evaluate their antioxidant capacity.

The absorbance of the test solution, control solution and blank solution at 517 nm was measured with a microplate reader. According to the linear regression equation of response obtained from the vitamin C standard curve, the DPPH radical scavenging

abilities of different samples were calculated, which were expressed as vitamin C equivalent (VCE). Then, the inhibition rate of the sample was obtained from the Equation 2.

$$\frac{DPPH \text{ scavenging capacity } (\%) = \frac{VCE \text{ amount of control} - VCE \text{ amount of sample}}{VCE \text{ amount of control}} \times 100}{\text{Eq. 2}}$$

Ferric reducing antioxidant capacity assurance, FRAP:  $Fe^{3+}$  and 2,4,6-Tri(2-pyridyl)-s-triazine (TPTZ) form a yellow chelate  $Fe^{3+}$ -TPTZ. Under acidic conditions,  $Fe^{3+}$ -TPTZ can be reduced by antioxidants to generate blue  $Fe^{2+}$ -TPTZ with maximum absorption at 593 nm. The formation amount of detected blue  $Fe^{2+}$ -TPTZ can reflect the reducing ability of the test sample, that is, the total antioxidant capacity of the sample. The standard curve was drawn with ferrous ferric oxide ( $Fe_3O_4$ ) as the standard solution, and the corresponding concentration of  $Fe_3O_4$  (mmol/L) was calculated on the standard curve according to the absorbance value after the reaction. The oxidation resistance (FRAP value) of the sample is expressed as the ratio of the  $FeSO_4$  concentration to the sample concentration required to achieve the same absorbance.

The absorbance was measured at 593 nm using a microplate reader. Iron reducing activity is expressed as vitamin C equivalent (VCE) antioxidant capacity in  $\mu\text{g}/\mu\text{g}$  dry weight.

#### **In vitro release assay and release mechanism study**

2 mL of B2-3'-G and ALG/CS-B-NPs sample solution (1 mg/mL) was accurately measured and placed into a dialysis bag (with molecular weight cut-off of 8,000–10,000) in a small beaker containing 15 mL of release medium (SIF or SGF) for reaction in a shaking table with a constant temperature water bath at 37 °C (100 rpm). Samples of 1 mL were taken at 0.25, 0.5, 0.75, 1, 2, 3, 4, 6, 8, 10, 12 and 24 h. After each sampling, 1 mL of release medium was added at the same time. The collected samples were passed through a 0.22  $\mu\text{m}$  microporous membrane, and then the absorbance was measured by enzyme-labeled instrument. The Equation 3 for Qn% of the cumulative release of B2-3'-G was as follows.

$$Qn\% = (C_n V + \sum_{i=1}^{n-1} C_i V_i) / M \quad \text{Eq. 3}$$

Where Qn% is the cumulative percent released of the drug at time N;  $C_n$  is the concentration of each B2-3'-G calculated from the  $n^{\text{th}}$  sampling; V is the total volume of SIF and SGF in the beaker;  $V_i$  is the volume of each sample at different time points; M is the mass of B2-3'-G contained in the dialysis bag.

B2-3'-G *in vitro* release mechanisms were studied by several drug release mathematical models, including zero-order, first-order, Korsmeyer-Peppas and

Higuchi models. Regression analysis was performed to select the best model according to the maximum of the determination coefficient ( $R^2$ ) indicating the best fit of the release data to linear regression.

#### **Cell culture**

HepG2 cells were purchased from the cell bank of the Type Culture Bank of the Chinese Academy of Sciences. The cells were cultured in Dulbecco's modified Eagle's medium supplemented with 10% fetal bovine serum, 100 IU/mL penicillin, and 100  $\mu\text{g}/\text{mL}$  streptomycin at 37 °C under 5% carbon dioxide ( $CO_2$ ) atmosphere.

#### **Cytotoxicity study**

Cells were pretreated with different concentrations of free B2-3'-G, B2-3'-G loaded nanoparticles (2.5, 5 and 10  $\mu\text{M}$ ) and blank nanoparticles, and incubated for 24 hours. Subsequently, the cells were washed twice with PBS and incubated again with MTT (0.5 mg/mL) for 4 hours. The formazan precipitate was dissolved in 150  $\mu\text{L}$  DMSO and the absorbance was measured at 490 nm using a Tecan Infinite M200 microplate reader (Das *et al.*, 2020).

#### **Cellular uptake study**

HepG2 was inoculated at a density of  $5 \times 10^4$  cells/well into a 6-well plate pre-coverslip, and incubated in a 37 °C, 5% carbon dioxide incubator for 24 h followed by the addition of FITC-labeled nanoparticles (10  $\mu\text{M}$ ) to the cells for 1, 2, and 4 h. Subsequently, the culture dish was taken out, rinsed twice with PBS, and the cells were fixed with 4% paraformaldehyde for 30 min. After rinsed twice with PBS, the nuclei were stained with 0.5  $\mu\text{g}/\text{mL}$  DAPI for 5 min, and then rinsed three times with PBS. The cover slip was removed and a drop of anti-fluorescence quenching agent was added. It was inverted onto the slide and labelled accordingly. After drying, fluorescence imaging of FITC was recorded using a fluorescence inverted microscope.

#### **The protective effects of B2-3'-G and ALG/CS-B-NPs on cells**

To investigate the protective effects of free B2-3'-G, ALG/CS-B-NPs and blank nanoparticles on  $H_2O_2$ -induced cytotoxicity, cells were seeded on 96-well plates at a density of  $5 \times 10^4$  cells/well and incubated for 24 h. Thereafter, the cells were washed with PBS and pre-treated with samples at three different concentrations (2.5, 5 and 10  $\mu\text{M}$ ) for 24 h, and then treated with  $H_2O_2$  (600  $\mu\text{M}$ ) for another 12 h. Subsequently, MTT (0.5 mg/mL) was added to cell culture plates and cultured for 4 h, and the absorbance measured at 490 nm using a Tecan Infinite M200 microplate reader (Chang *et al.*, 2021; He *et al.*, 2021).

## Statistical analysis

Statistical analysis of three independent replicates was performed. The data were presented as mean and standard deviation (SD). The results were calculated, and graphs were plotted via Origin software (version 9.1). GraphPad Prism 5.0 software was used for one-way analysis of variance to determine the significance of the difference, and  $p < 0.05$  indicated that the difference was statistically significant.

## RESULTS AND DISCUSSION

### Preparation of ALG/CS-B-NPs

As shown in Table I, the nanoparticle (ALG/CS ratio=1.2) with B2-3`-G and without B2-3`-G exhibited an average diameter of 178 and 201 nm, respectively. Zeta potential was negative and did not

change significantly with the encapsulation of B2-3`-G. This negative value can be explained by the higher concentration of ALG than CS. Table I shows that the average zeta potential did not change significantly and the particle size increased slightly from 178 nm to 201nm after encapsulation of B2-3`-G. However, the EE of B2-3`-G in nanoparticles (ALG/CS ratio = 1.2) was only 1.43% (Marcato *et al.*, 2013).

When nanoparticles with ALG/CS ratio of 0.2 were prepared in the presence and absence of B2-3`-G, the particle sizes were 169 nm and 160 nm, respectively, and the zeta potential were +33.5 (with B2-3`-G) and +27.2 mV (without B2-3`-G). The positive potential indicated that chitosan existed on the surface of the particles. Compared with the nanoparticles when the ALG/CS ratio was 1.2, the electronic efficiency of the nanoparticles was improved to 80.25%.

Table I

Zeta potential (surface charge), particles sizes, and encapsulation efficiency of Alginate/Chitosan nanoparticles in two different ratios with and without B2-3`-G

ALG/CS ratios	B2-3`-G (mg)	Size (nm)	PDI	Zeta potential (mV)	EE (%)
0.20	0	160.1 ± 1.3	0.334 ± 0.022	+27.2 ± 0.9	-
0.20	9	169.2 ± 0.9	0.312 ± 0.019	+33.5 ± 0.8	80.25 ± 2.50
1.20	0	178.2 ± 1.2	0.276 ± 0.021	-13.5 ± 1.2	-
1.20	9	201.1 ± 1.1	0.285 ± 0.017	-17.2 ± 1.1	1.43 ± 0.65

### Morphology study of nanoparticles by TEM

The morphology of the nanoparticles was investigated using TEM. TEM image (Figure 1) revealed that the nanoparticles exhibited a regular spherical shape, good uniformity and dispersibility, and no adhesion phenomenon. The small black dots adhered to the surface of the nanoparticles may be free B2-3`-G. The results reported by Xiong *et al.* (2016) also showed nanoparticles with spherical shape and uniform size.

### FTIR analysis

As shown in Figure 2, the physical mixture was basically the overlap of the peaks. The main absorption peak of B2-3`-G in the physical mixture was not significantly changed in the characteristic region of 4000-1300  $\text{cm}^{-1}$ , while the characteristic peak of B2-3`-G in B2-3`-G-CS/AL-NPs was shifted and weakened in the characteristic region of 4000-1300  $\text{cm}^{-1}$ , and some characteristic peaks

disappeared in the fingerprint region of 1300 -500  $\text{cm}^{-1}$ .

Typically, the major functional groups in ALG are -OH, C=O, and C-O; the major functional groups in CS are -OH, C-O, and -NH; and the major functional groups in B2-3`-G are -OH, C-O, C=C, and C=O. These similar functional groups are distributed in the same region, but they can resonate with each other. As a result, the intensity of the vibration in the FTIR spectrum of the B2-3`-G-loaded nanoparticles was higher than that of CS, ALG, B2-3`-G, or the empty nanoparticles (Luong *et al.*, 2021).

The typical characteristic peak spectra of O-H, C=C, and C-O with strong and broad peaks appeared in B2-3`-G at 3399 $\text{cm}^{-1}$ , 1600-1450  $\text{cm}^{-1}$ , and 1241 $\text{cm}^{-1}$ , respectively. From the position data of some main vibrations in the infrared spectrum of the B2-3`-G-loaded nanoparticles, it could be seen that the vibrations of these main characteristic peaks in the B2-3`-G-loaded nanoparticles were slightly shifted than the free B2-3`-G. These results could indicate

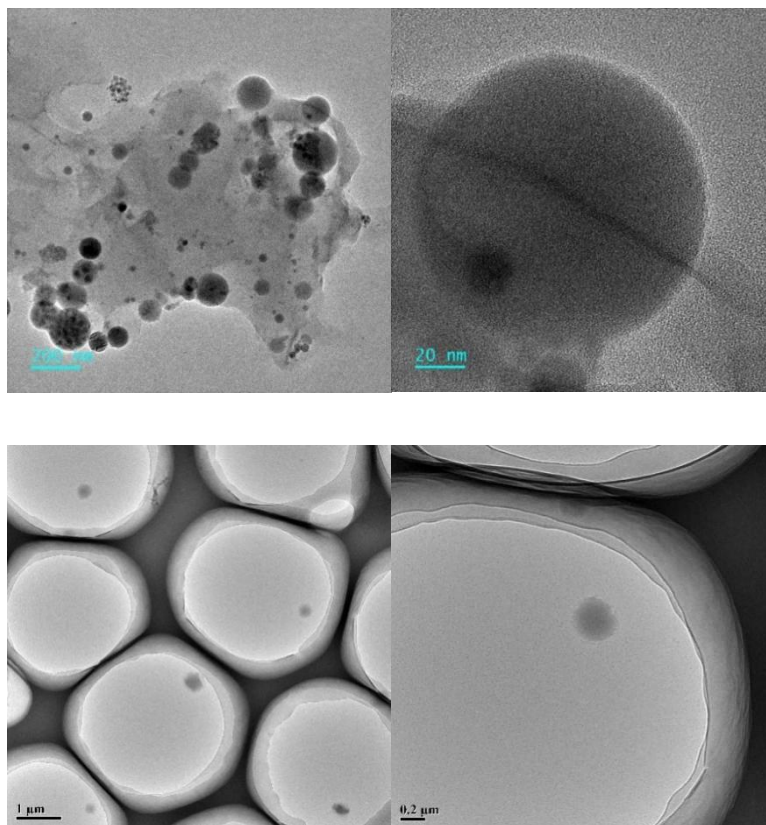


**Figure 1.** TEM image of ALG/CS-B-NPs

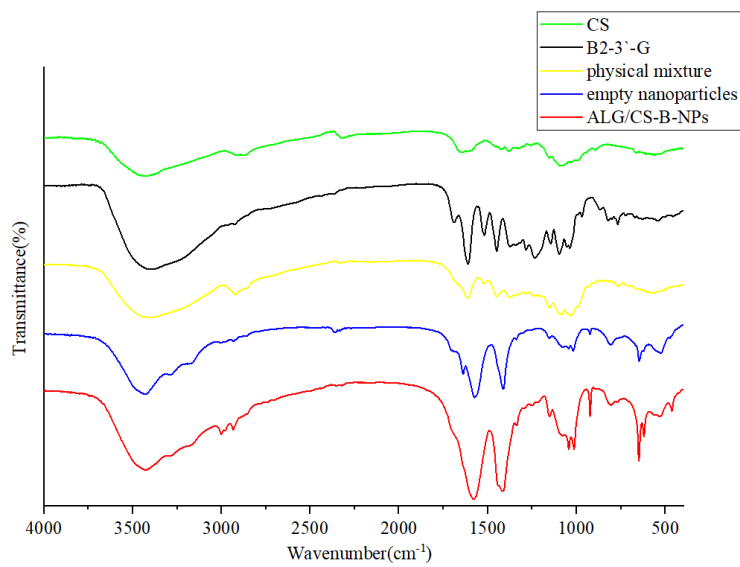


**Figure 2.** Fourier transform infrared (FTIR) spectra of B2-3'-G, CS, physical mixture, empty nanoparticles and ALG/CS-B-NPs.

that ALG, CS, and B2-3'-G can interact through their hydroxyl, carbonyl, and amine groups (Xiong *et al.*, 2016).

The above outcomes showed that in the process of preparing the nanoparticles by the ion gel method, CS and ALG could form a nanogel complex loaded with B2-3'-G in the solution through the anion and cation groups they respectively carried. The basic chemical structures of each substance were not fundamentally changed, no new chemical bonds were formed, and the formed complex was not a new compound. It could be suggested that there might be

hydrogen bonds or van der Waals forces between B2-3'-G and CS and ALG.

### XRD analysis

Figure 3 unveils that B2-3'-G was in an amorphous state. When these three substances were physically mixed, the crystal diffraction peaks for CS and ALG did not change. However, after the embedding with the ion crosslinking method, more crystal diffraction peaks at different positions were generated, suggesting that B2-3'-G might have hydrogen bonds or van der Waals forces bonded with the embedding material (Thomas *et al.*, 2020; Soltanzadeh *et al.*, 2021).

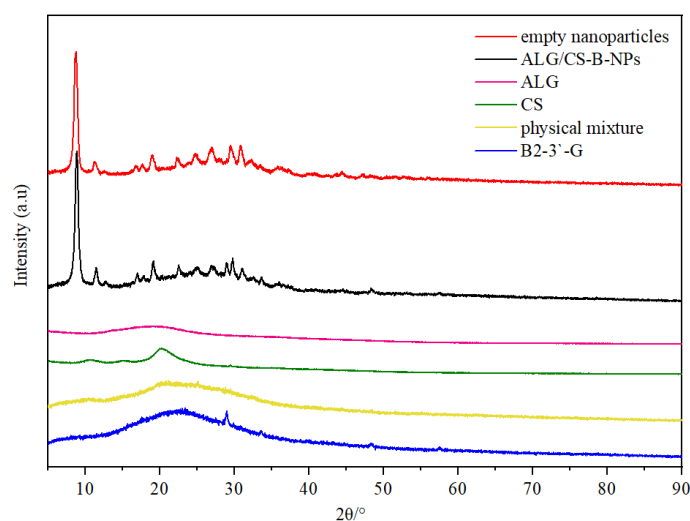


**Figure 3.** XRD patterns of B2-3'-G, CS, ALG, physical mixture, empty nanoparticles and ALG/CS-B-NPs.

### TG-DSC analysis

When the guest molecule B2-3'-G was embedded in the embedding material, its melting point, boiling point, or heating point would usually change, thus proving the formation of the clathrate. Figure 4 shows that B2-3'-G has a mass loss (10%) within 10-100 °C, probably due to the small amount of moisture, and when the temperature rises to 150-300 °C, the thermal decomposition of the B2-3'-G results in a significant mass loss (29%). ALG/CS-NPs (empty nanoparticles) and ALG/CS-B-NPs exhibited a flatter TG curve with less mass loss (20%) between 0 and 300 °C. These results indicate that the ALG/CS-B-NPs had a protective effect on the B2-3'-G substance and could improve its thermal stability (Soltanzadeh *et al.*, 2021). DSC results showed that B2-3'-G had a melting endotherm at 172 °C, while B2-3'-G had no melting endotherm in either the ALG/CS-NPs or ALG/CS-B-NPs, suggesting that B2-3'-G was well embedded in the nanoparticles.

### Antioxidant result before and after simulate gastrointestinal digestion

The antioxidant activities of ALG/CS-B-NPs and free B2-3'-G were examined and compared before and after gastrointestinal digestion. As shown in the Figure 5, undigested B2-3'-G exhibited greater DPPH antioxidant activity and iron reducing activity than digested B2-3'-G. Undigested ALG/CS-B-NPs had lower antioxidant activity than undigested free B2-3'-G, possibly because B2-3'-G was protected by the encapsulation of ALG and CS at this time and was unable to interact with the reagents, and the antioxidant activity exhibited at this time might be due to the small amount of B2-3'-G and the carrier material attached to the carrier surface.

After gastrointestinal digestion with B2-3'-G, the DPPH free radical scavenging and iron reducing activities were significantly reduced; DPPH free radical scavenging capacity decreased by 60% and iron reducing capacity decreased by 37%. ALG/CS-

B-NPs had nearly twice the DPPH radical scavenging capacity and more than twice the iron reducing capacity after gastrointestinal digestion than before gastrointestinal digestion. B2-3'-G may decompose and gradually inactivate after digestion under gastrointestinal conditions. However, B2-3'-G in ALG/CS-B-NPs began to slowly release in large amounts after digestion under gastrointestinal conditions. Before this, B2-3'-G was protected by

ALG and CS to reduce the influence of external conditions. The supporting material may possess certain antioxidant activity. The results are consistent with other studies.

Therefore, this study demonstrated that ALG/CS-B-NPs had an advantage over free B2-3'-G when digested in the gastrointestinal tract, effectively protecting B2-3'-G from external conditions and retaining its antioxidant activity.

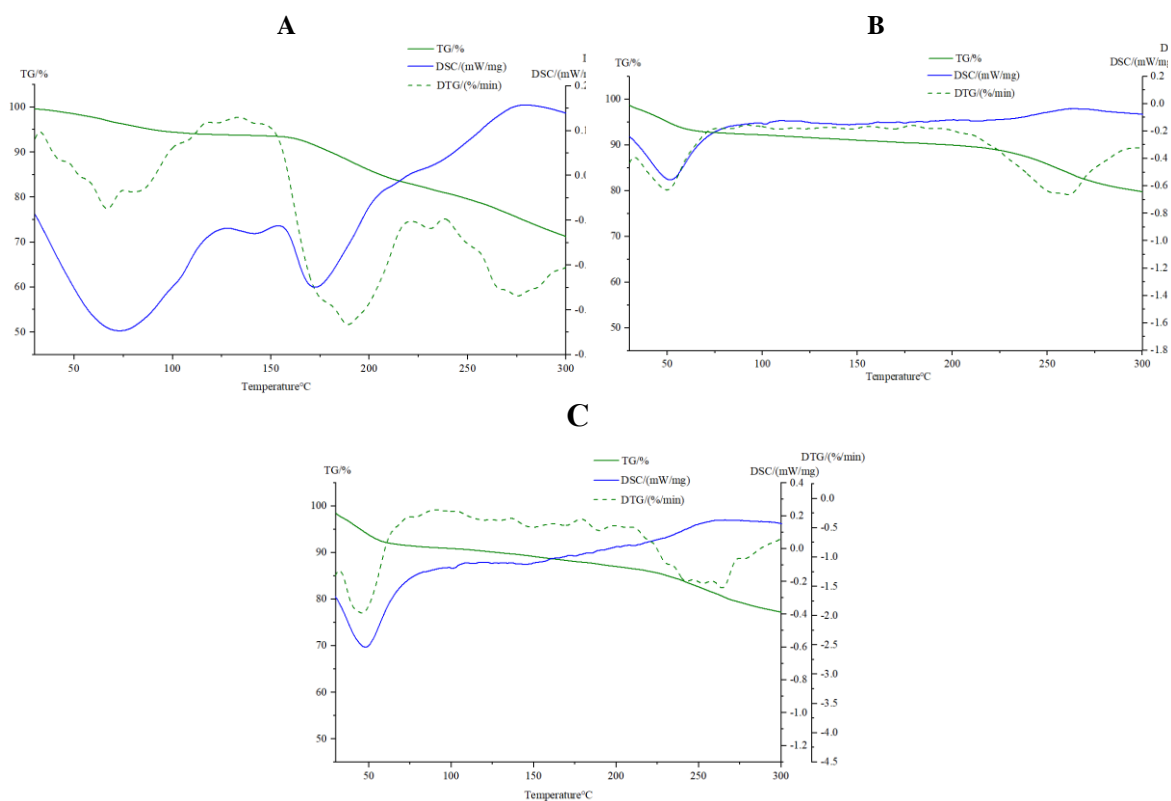


**Figure 4.** Thermogravimetric curve diagram of A: B2-3'-G, B: ALG/CS-NPs, C: ALG/CS-B-NPs.

### ***In vitro* release of B2-3'-G**

The *in vitro* release behavior of B2-3'-G and ALG/CS-B-NPs was studied at 37 °C in SGF and SIF. Figure 6 reveals that the cumulative release rate of free B2-3'-G in SGF and SIF at the first 4h is 99%; ALG/CS-B-NPs, on the other hand, showed sustained release in both SGF and SIF, with cumulative release rates of 75% and 82% at 24 h, respectively. In the previous hour, ALG/CS-B-NPs had an initial explosive release of B2-3'-G in both media, up to 37% of the cumulative release, which could be due to the instantaneous diffusion of B2-3'-

G attached to the surface layer of the nanoparticles, followed by rapid hydration of the nanoparticles due to the hydrophilicity of ALG and CS. The cumulative release rate of B2-3'-G in ALG/CS-B-NPs in SGF was lower than that in SIF, probably because the protonation of chitosan amine groups limited the diffusion of B2-3'-G in solution under acidic conditions. These results indicate that after the complete release of B2-3'-G adsorbed on the surface of ALG/CS-B-NPs, the following substances will be released continuously and slowly from inside the nanoparticles (Shishir *et al.*, 2019).

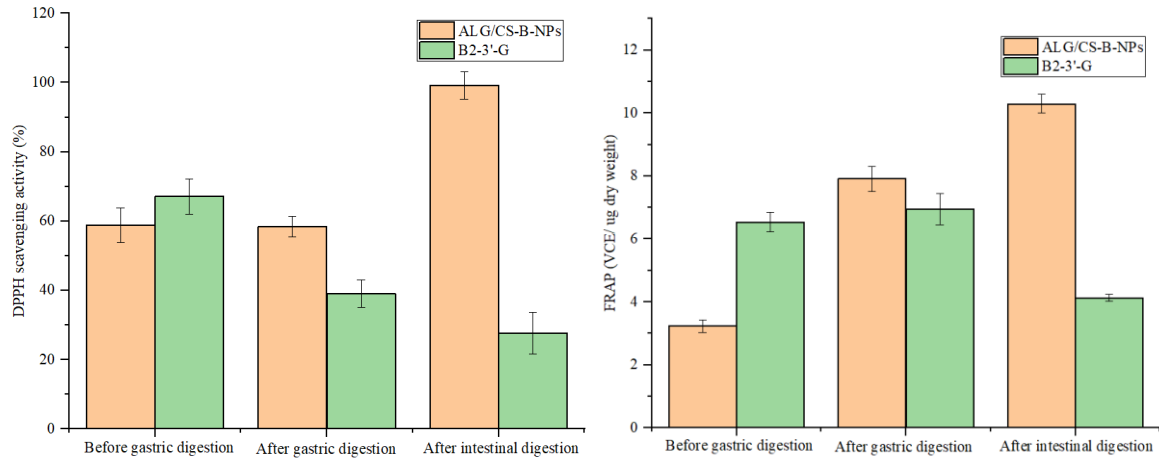


Figure 5. DPPH scavenging activity and FRAP activity.

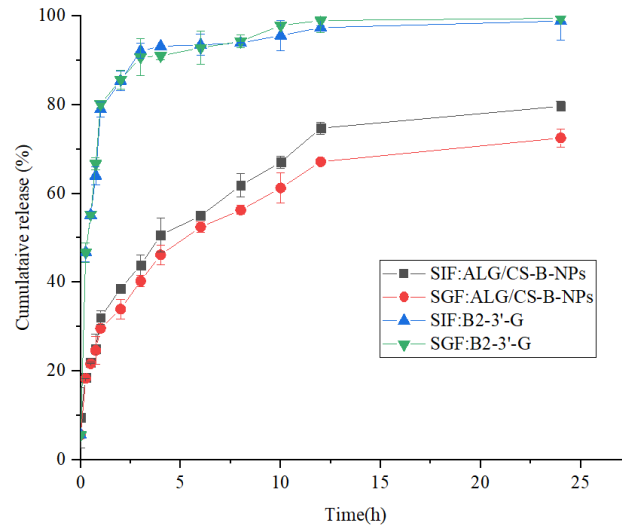


Figure 6. Release behavior of free B2-3'-G and B2-3'-G from ALG/CS-B-NPs in gastro-intestinal condition.

### B2-3'-G release mechanism study

Drug release mechanism refers to the process of drug release from preparations, which can be divided into several pathways, such as diffusion, dissolution or melting, fragmentation, swelling, erosion and degradation. The final release mechanism depends on the nature of the core and carrier systems, the environment, and factors associated with the process.

The release behavior of ALG/CS-B-NPs in SGF and SIF was studied, and the release amounts at different time points were measured. Then the experimental data were fitted by nonlinear regression method, and the release kinetics model was analyzed. Table II shows that the release of B2-3'-G in SGF followed

the Higuchi model ( $R^2 > 0.96$ ) and the release rate decreased over time, indicating that the diffusion of nanoparticles was hindered by the drug loading layer. The release in SIF was consistent with the Korsmeyer-Peppas model ( $R^2 > 0.99$ ), and when  $n < 0.45$ , it belonged to Fick diffusion. The release rate increased over time, proving that the diffusion of nanoparticles was promoted by the drug loading layer. This may be related to the swelling property and stability of the nanoparticles in different media. The experimental results provide a theoretical basis for drug delivery and controlled release of nanoparticles in the digestive tract (Li *et al.*, 2018; Shishir *et al.*, 2020).

**Table II**

Model fitness of B2-3`-G and ALG/CS-B-NPs *in vitro* gastrointestinal digestion

	Release model	Model equation	ALG/CS-B-NPs	
			R <sup>2</sup>	n
(a) Models SGF	Zero order	M0-Mt=kt	0.6237	-
	First order	In Mt=In M0+kt	0.8703	-
	Higuchi	M0-Mt=kt <sub>1/2</sub>	0.9659	-
	Korsmeyer-Peppas	log(M0-Mt)=log k+n log t	0.8911	0.32572 ± 0.0552
(b) Models SIF	Zero order	M0-Mt=kt	0.7931	-
	First order	In Mt=In M0+kt	0.8849	-
	Higuchi	M0-Mt=kt <sub>1/2</sub>	0.9741	-
	Korsmeyer-Peppas	log(M0-Mt)=log k+n log t	0.9900	0.35436 ± 0.0093

**Effect of B2-3`-G and B2-3`-G-loaded NPs on cell activity**

The results of the activity of B2-3`-G and ALG/CS-B-NPs on HepG2 cells showed that when 10 - 100 µg/mL B2-3`-G was applied to cells for 24 h, the activity proliferate significantly, compared with the blank control group (p<0.01) - Figure 7. There was no significant change in cell activity compared with the control group, when the cells were treated with ALG/CS-B-NPs below 100 µg/mL (p>0.05). It suggested that the ALG/CS-B-NPs had no significant toxicity to cells at a concentration below 100 µg/mL. The blank NPs group also indicate no change in cellular activity. Therefore, the maximum

concentration of B2-3`-G in subsequent experiments was 10 µg/mL.

**Cellular uptake study**

In order to observe the uptake of nanoparticles by cells, the intracellular fluorescence of FITC-labeled nanoparticles were cultured with HepG 2 cells for 1, 2 and 4 h, then observed under a fluorescence inversion microscope. As shown in Figure 8, the uptake of nanoparticles by cells was time-dependent. With the increase of incubation time, the uptake of cells was increased and the fluorescence signal was enhanced. This indicates that ALG/CS-B-NPs nanoparticles could be used as a carrier for B2-3'-G by enhancing uptake by HepG2 cells.

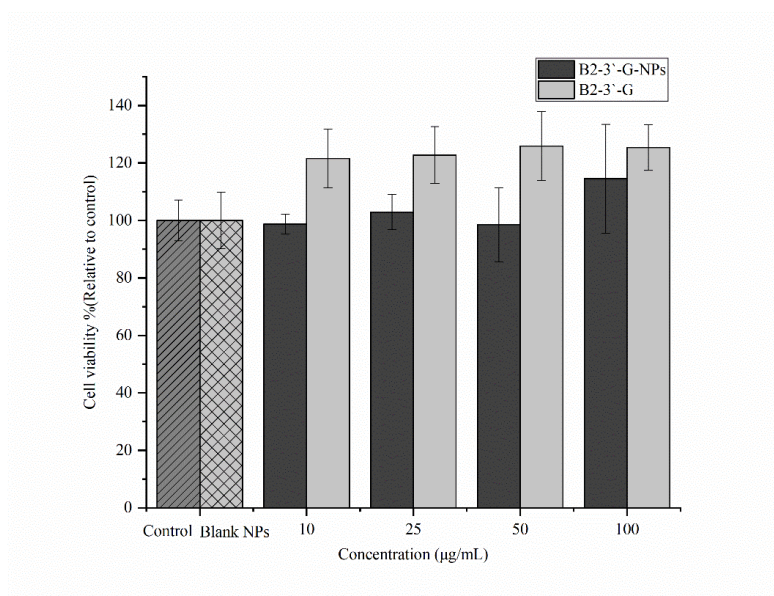


**Figure 7.** Effect of B2-3`-G and ALG/CS-B-NPs on the viability of HepG2 cell.

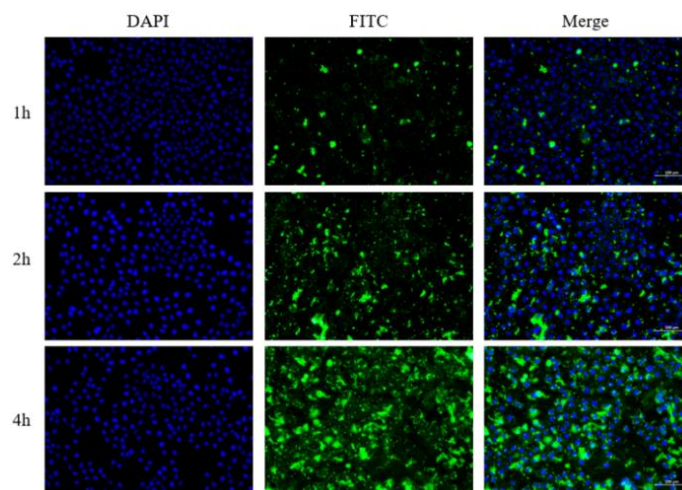


**Figure 8.** Uptake of FITC-labeled nanoparticles in HepG2 cells after incubation for 1, 2 and 4 h (scale length: 100  $\mu$ m).

### Effect of B2-3'-G and B2-3'-G-loaded NPs on H<sub>2</sub>O<sub>2</sub>-induced cytotoxicity in human HepG2 cells

Figure 9 reveals that HepG2 cell activity gradually weakened with the increase of concentration, showing a concentration-dependent manner, after treating with H<sub>2</sub>O<sub>2</sub> for 12 h. When the concentration of H<sub>2</sub>O<sub>2</sub> reached 600  $\mu$ M, the activity of HepG2 cells was reduced to  $47.5 \pm 1.0\%$ . Therefore, a model of oxidative stress injury in HepG2 cells induced by 600  $\mu$ M H<sub>2</sub>O<sub>2</sub> was established (Chang *et al.*, 2021).

Three concentrations of B2-3'-G were set: 2.5, 5, and 10  $\mu$ g/mL. Figure 10 shows that a significant difference between the H<sub>2</sub>O<sub>2</sub> group and the blank control group ( $p < 0.01$ ) existed. Compared with the H<sub>2</sub>O<sub>2</sub> group, B2-3'-G group, blank NPs group and ALG/CS-B-NPs group all had antioxidant and pre-

protective effects on cells, which reduced apoptosis after hydrogen peroxide injury. Compared with the H<sub>2</sub>O<sub>2</sub> group, cell viability was increased by 15% in the blank NPs group, by 19%, 20%, and 23% in the free B2-3'-G group, and by 32%, 35%, and 36% in the ALG/CS-B-NPs group; all the results had significant differences ( $p < 0.01$ ). It could be seen that the cell protection ability of ALG/CS-B-NPs was stronger than that of free B2-3'-G, which might be due to the anti-oxidation protection effect of the nanoparticles themselves, and the synergistic addition of anti-oxidation effect with B2-3'-G. It suggests that embedding B2-3'-G in the nanoparticles could exert a better anti-oxidation effect (Tzankova *et al.*, 2017).

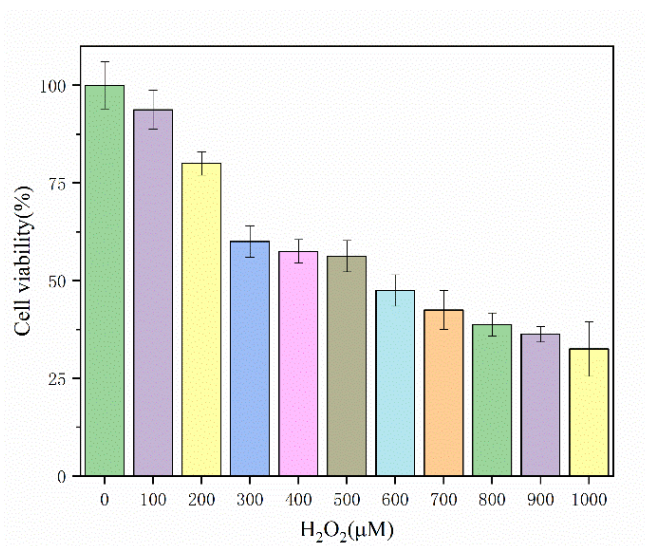


**Figure 9.** Effect of hydrogen peroxide on proliferation of HepG2 cells under different concentration.

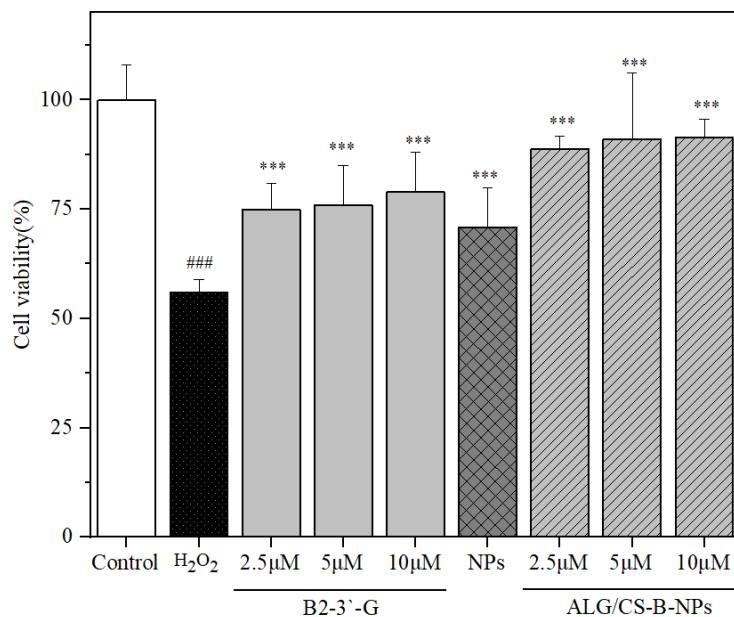


**Figure 10.** Protective effects of B2-3'-G on H<sub>2</sub>O<sub>2</sub>-induced oxidative damage in HepG2 cells. ###p < 0.01 versus control group; \*\*\*p < 0.01 vs. H<sub>2</sub>O<sub>2</sub> group.

## CONCLUSIONS

In this study, ALG/CS-B-NPs were first prepared by ion crosslinking method. The results showed that B2-3'-G was well encapsulated in the nanoparticles, and the stability of the compounds was improved. In the simulated gastrointestinal digestion, ALG/CS-B-NPs showed sustained release and protective effects. In particular, the *in vitro* experiments demonstrated that B2-3'-G loaded in nanoparticles could significantly protect HepG2 cells and reduce H<sub>2</sub>O<sub>2</sub>-induced cytotoxicity. In conclusion, B2-3'-G nanoparticles are effective loaded nanoparticles, which can achieve the sustained release of B2-3'-G and make it have higher biological activity. The proposed methodology will be a useful tool for improving the physicochemical and functional properties of grape seed galloylated procyanidins, which provides scientific support for the potential application of these bioactive compounds in the food and pharmaceutical field.

**CONFLICTS OF INTEREST:** The authors declare no conflict of interest.

## REFERENCES

Agarwal C., Veluri R., Kaur M., Chou S.C., Thompson J. A., Agarwal R., 2007. Fractionation of high molecular weight tannins in grape seed extract and identification of procyanidin B2-3,3'-di-O-gallate as a major active constituent causing

growth inhibition and apoptotic death of DU145 human prostate carcinoma cells. *Carcinogenesis*, **28**, 1478–1484.

Bitzer Z.T., Glisan S.L., Dorenkott M.R., Goodrich K.M., Ye L., O'Keefe S.F., Lambert J.D., Neilson A.P., 2015. Cocoa procyanidins with different degrees of polymerization possess distinct activities in models of colonic inflammation. *J Nutr Biochem.*, **26**, 827–831.

Chang X., Dong S., Bai W., Di Y., Gu R., Liu F., Zhao B., Wang Y., Liu X., 2021. Methylated Metabolites of Chicoric Acid Ameliorate Hydrogen Peroxide (H<sub>2</sub>O<sub>2</sub>)-Induced Oxidative Stress in HepG2 Cells. *J. Agric. Food Chem.*, **69**, 2179–2189.

Das G., A., Patra J.K., A., Shin H.-S., 2020. Biosynthesis, and potential effect of fern mediated biocompatible silver nanoparticles by cytotoxicity, antidiabetic, antioxidant and antibacterial, studies. *Mater. Sci. Eng. C.*, **114**, 111011.

Ezzat H.M., Elnaggar Y., Abdallah O.Y., 2019. Improved oral bioavailability of the anticancer drug catechin using chitosomes: Design, in-vitro appraisal and in-vivo studies. *Int.J.Pharm.*, **565**, 488–498.

Gao Y., Wu Y., 2022. Recent advances of chitosan-based nanoparticles for biomedical and biotechnological applications. *Int. J. Biol. Macromol.*, **203**, 379–388.

He S., Cui X., Khan A., Liu Y., Wang Y., Cui Q., Zhao T., Cao J., Cheng G., 2021. Activity Guided Isolation of Phenolic Compositions from *Anneslea fragrans* Wall and Their Cytoprotective Effect against Hydrogen Peroxide Induced Oxidative Stress in HepG2 Cells. *Molecules*, **26**, 3690.

Hua Y., Wei Z., Xue C., 2021. Chitosan and its composites-based delivery systems: advances and applications in food science and nutrition sector. *Crit Rev Food Sci Nutr.*, **18**, 1–20.

- Jadach B., Świetlik W., Froelich A., 2022. Sodium Alginate as a Pharmaceutical Excipient: Novel Applications of a Well-known Polymer. *J. Pharm Sci.*, **111**, 1250–1261.
- Karavelioglu Z., Cakir-Koc R., 2021. Preparation of chitosan nanoparticles as Ginkgo Biloba extract carrier: *In vitro* neuroprotective effect on oxidative stress-induced human neuroblastoma cells (SH-SY5Y). *Int. J. Biol. Macromol.*, **192**, 675–683.
- Li F., Jin H., Xiao J., Yin X., Liu X., Li D., Huang Q., 2018. The simultaneous loading of catechin and quercetin on chitosan-based nanoparticles as effective antioxidant and antibacterial agent. *Food Res Int.*, **111**, 351–360.
- Lopes M., Aniceto D., Abrantes M., Simões S., Branco F., Vitória I., Botelho M.F., Seça R., Veiga F., Ribeiro, A., 2017. In vivo biodistribution of antihyperglycemic biopolymer-based nanoparticles for the treatment of type 1 and type 2 diabetes. *Eur J Pharm Biopharm.*, **113**, 88–96.
- Luo L., Cui Y., Cheng J., Fang B., Wei Z., Sun B., 2018. An approach for degradation of grape seed and skin proanthocyanidin polymers into oligomers by sulphurous acid. *Food Chem.*, **256**, 203–211.
- Luong P.H., Nguyen T.C., Pham T.D., Tran D.M.T., Ly T.N.L., Vu Q.T., Tran T.K.N., Thai H., 2021. Preparation and Assessment of Some Characteristics of Nanoparticles Based on Sodium Alginate, Chitosan, and *Camellia chrysantha* Polyphenols. *Int J Polym Sci.*, **2021**, (5581177), 1–11.
- Marcato P.D., Adami L.F., Barbosa R.D., Melo P.S., Ferreira I., Paula L.B., Durán N., Seabra A.B., 2013. Development of a Sustained-release System for Nitric Oxide Delivery using Alginate/Chitosan Nanoparticles. *Curr Nanosci.*, **9**, 1–7.
- Rajapaksha D., Shimizu N., 2020. Valorization of spent black tea by recovery of antioxidant polyphenolic compounds: Subcritical solvent extraction and microencapsulation. *Food Sci. Nutr.*, **8**, 4297–4307.
- Sathiyaseelan A., Saravanakumar K., Jayalakshmi J., Gopi M., Shajahan A., Barathikannan K., Kalaichelvan P.T., Wang M.H., 2020. Trigone-line-loaded chitosan nanoparticles prompted antitumor activity on glioma cells and biocompatibility with pheochromocytoma cells. *Int. J. Biol. Macromol.*, **163**, 36–43.
- Shishir M.R., Karim N., Gowd V., Xie J., Zheng X., Chen W., 2019. Pectin-chitosan conjugated nanoliposome as a promising delivery system for neohesperidin: Characterization, release behavior, cellular uptake, and antioxidant property. *Food Hydrocoll.*, **95**, 432–444.
- Shishir M., Karim N., Xie J., Rashwan A.K., Chen W., 2020. Colonic delivery of pelargonidin-3-O-glucoside using pectin-chitosan-nanoliposome: Transport mechanism and bioactivity retention. *Int. J. Biol. Macromol.*, **159**, 341–355.
- Soltanzadeh M., Peighambaroust S.H., Ghanbarzadeh B., Mohammadi M., Lorenzo J.M., 2021. Chitosan nanoparticles encapsulating lemongrass (*Cymbopogon commutatus*) essential oil: Physicochemical, structural, antimicrobial and in-vitro release properties. *Int. J. Biol. Macromol.*, **192**, 1084–1097.
- Suda M., Katoh M., Toda K., Matsumoto K., Kawaguchi K., Kawahara S., Hattori Y., Fujii H., Makabe H., 2013. Syntheses of procyanidin B2 and B3 gallate derivatives using equimolar condensation mediated by Yb(OTf)<sub>3</sub> and their antitumor activities. *Bioorganic Med. Chem. Lett.*, **23**, 4935–4939.
- Sun B.S., Ricardo-da-Silva J.M., Spranger M.I., 2001. Quantification of catechins and proanthocyanidins in several Portuguese grapevine varieties and red wines. *Ciência Téc. Vitiv.*, **16**, 23–34.
- Sun B.S., Spranger M.I., 2005. Review: quantitative extraction and analysis of grape and wine proanthocyanidins and stilbenes. *Ciência Téc. Vitiv.*, **20**, 59–91.
- Thomas D., KurienThomas K., Latha M.S., 2020. Preparation and evaluation of alginate nanoparticles prepared by green method for drug delivery applications. *Int. J. Biol. Macromol.*, **154**, 888–895.
- Tyagi A., Raina K., Shrestha S.P., Miller B., Thompson J.A., Wempe M.F., Agarwal R., Agarwal C., 2014. Procyanidin B2 3,3(")-di-O-gallate, a biologically active constituent of grape seed extract, induces apoptosis in human prostate cancer cells via targeting NF-κB, Stat3, and AP1 transcription factors. *Nutr Cancer.*, **66**, 736–746.
- Tzankova V., Aluani D., Kondeva-Burdina M., Yordanov Y., Odzhakov F., Apostolov A., Yoncheva K., 2017. Hepatoprotective and antioxidant activity of quercetin loaded chitosan/alginate particles *in vitro* and in vivo in a model of paracetamol-induced toxicity. *Biomed. Pharmacother.*, **92**, 569–579.
- Xiong W., Li L., Wang Y., Yu Y., Wang S., Gao Y., Liang Y., Zhang G., Pan W., Yang X., 2016. Design and evaluation of a novel potential carrier for a hydrophilic antitumor drug: Auricularia auricular polysaccharide-chitosan nanoparticles as a delivery system for doxorubicin hydrochloride. *Int. J. Pharm.*, **511**, 267–275.